Chapter 2 Design

The basic principle of an electrostatic vibration-to-electricity converter is to increase the electric potential across a capacitor by the movement of a charged object in electric field, and therefore increase the stored energy. For converters constructed with variable capacitors, the charged object is the movable electrode driven by vibration, and the output is the net electric energy produced in the transduction process.

The operation and device modeling are discussed in this chapter. Characterization of common low-level vibrations is also included. Finally, device design and simulation are presented.

2.1 Principle

The basic component of an electrostatic energy converter is the variable capacitor. The movable structure in the variable capacitor, which will be fabricated by MEMS technology, is driven by mechanical vibrations and its capacitance varies between C_{max} and C_{min}

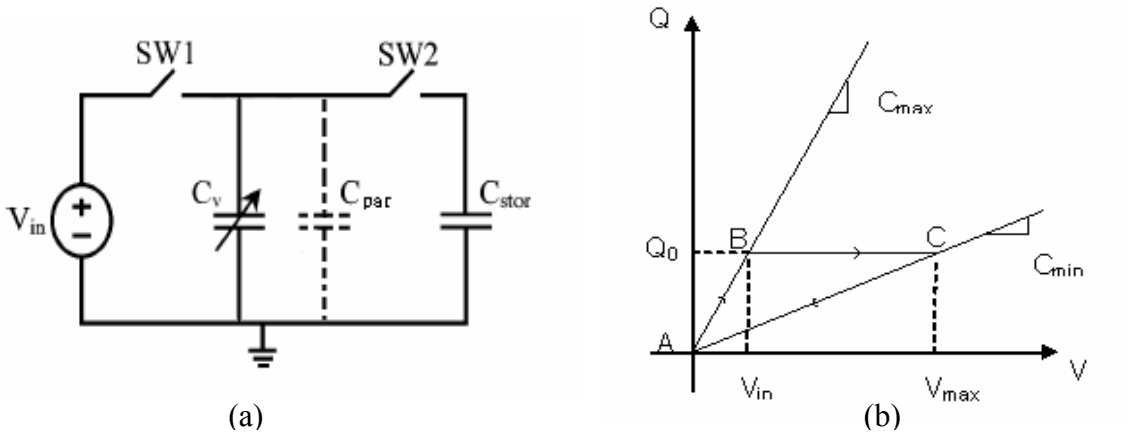

Figure 2.1 Principle of the electrostatic energy converter

As shown in Figure 2.1(a), the variable capacitor C_v is charged by an external voltage source V_{in} through the switch SW1 when the C_v is at its maximum $C_{max.}$ When C_v is charged to V_{in} (from A to B in Figure 2.1(b)), SW1 is open and then the capacitance is changed form C_{max} to C_{min} (B to C) due to the electrode displacement caused by vibration. In this process, the charge Q on the capacitor remains constant (SW1 and SW2 both open). Therefore, the terminal voltage on the capacitor is increased and the vibration energy is converted to the energy stored in the capacitor. When the capacitance reaches C_{min} (V_{max}), SW2 is closed and the charge is transferred to a storage capacitor or load (C to A). If complete discharge is assumed as shown in Figure 2.1(a), the area enclosed by the triangle ABC represents the net output energy, which can be expressed as

$$E = \frac{1}{2} V_{in}^{\ 2} (C_{max} - C_{min})(\frac{C_{max}}{C_{min}}) \tag{2.1a}$$

$$= \frac{1}{2} V_{max} V_{in} (C_{max} - C_{min}) \tag{2.1b}$$

In reality, there is a parasitic capacitance in MEMS structures and circuits. Thus Equation 2.1a can be modified to account for the parasitic capacitance C_{par},

$$E = \frac{1}{2} V_{in}^{\ 2} (C_{max} - C_{min})(\frac{C_{max} + C_{par}}{C_{min} + C_{par}}) \tag{2.1a'}$$

If the frequency of vibration is *f*, the capacitance varies between C_{max} and C_{min} with a frequency of *2f*. Therefore the output power is

$$P = E \times (2f) = f V_{in}^{\ 2} (C_{max} - C_{min})(\frac{C_{max} + C_{par}}{C_{min} + C_{par}}) \tag{2.2}$$

The actual displacemnet of the movable strutcure in the variable capacitor, and therefore the value of C_{max} and C_{min}, is determined by mechanical structural dynamics. This electro-mechanical dynamics of the conversion process can be modeled as a

spring-damper-mass system. As shown in Figure 2.2, y is the displacement of the vibration source, z is the reletive displacement between the movable electrode in the variable capacitor and the frame, m is the mass of the movable electrode, k is the spring constant, $b_m(z,\dot{z})$ is the equivalent mechanical damping representing energy loss caused mainly by fluidic damping, and b_e(z) is the equivalent electrical damping representing the energy converted into electricity. The dynamic equation of this system can be written as:

$$m\ddot{z} + b_e(z) + b_m(z,\dot{z}) + kz = -m\ddot{y} \tag{2.3}$$

Notice that the mechanical damping force, $b_m(z,\dot{z})$, is a function of both the displacement z of the shuttle mass and its velocity $\dot{z}$. The major contribute of this term is the squeeze film effect and the exact expression is structure dependent. The $b_e(z)$ term is the electrostaitc force induced on the MEMS structure. The capacitance of the MEMS variable capacitor at a given time t is determined by the displacement z of the shuttle mass.

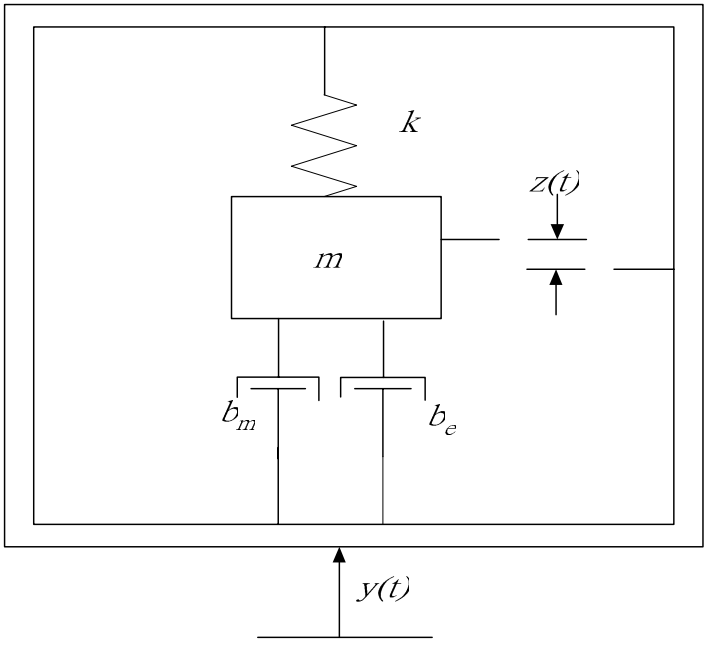

Figure 2.2 Schematic of the conversion dynamic model

For such a second order system, the system response reaches its maximum when excited at the resonant frequency. Thus, the system should be designed according to the characteristics of the vibration source which is discussed in the next section.

2.2 Characteristics of vibration

There are various kinds of vibrations in the environment; however, it is desired to target those most common ones in homes, office buildings, cars, and factories to maximize the potential applicability of the device. In order to estimate how much power can be converted from vibrations, the details of vibration characteristics must be considered.

Measurement of various vibration sources was conducted by Roundy [11], as shown in Figure 2.3. From the spectrum of these measured low-level vibrations, two conclusions can be drawn. First, the assumption of steady vibration concentrated at specific frequencies seems reasonable. Second, the higher frequency vibration modes are lower in acceleration magnitude than the low frequency fundamental mode.

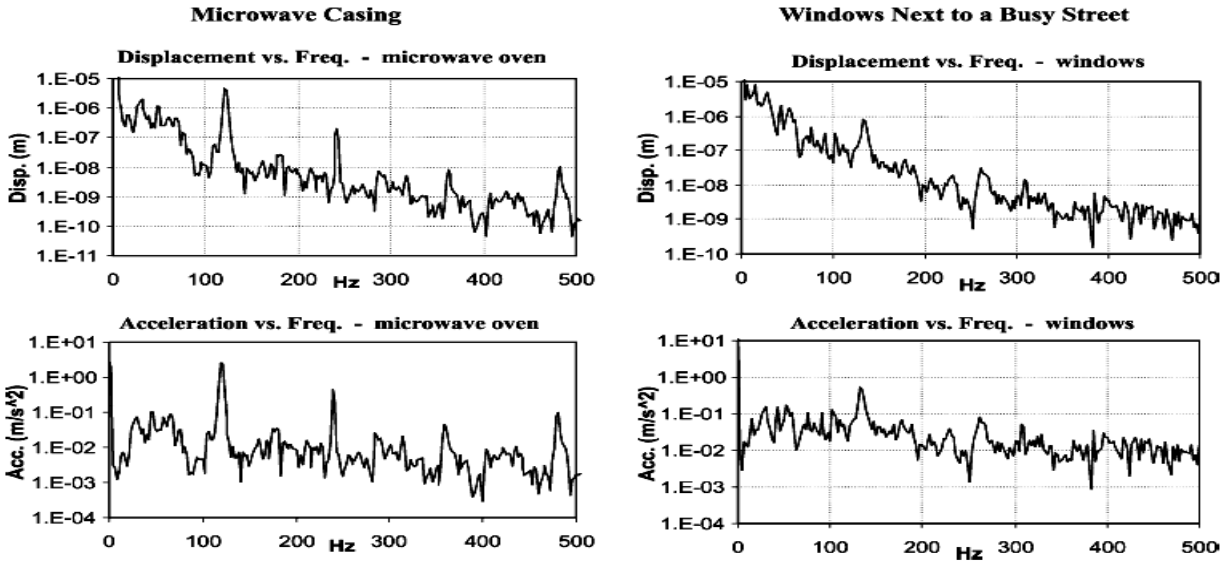

Figure 2.3 Vibration spectra by Roundy [11]

We have also measured a number of sources, as shown in Figure 2.4. The most energetic modes are the low-frequency ones, as observed by Roundy. From Figure 2.3 and 2.4, it is noticed that a general vibration, from the microwave oven or air conditioner, has a peak acceleration of about 2.25 m/s^2 at about 120 Hz. Therefore, the resonant frequency of the micro mechanical structure will be designed to match this vibration source for maximum displacement and power output.

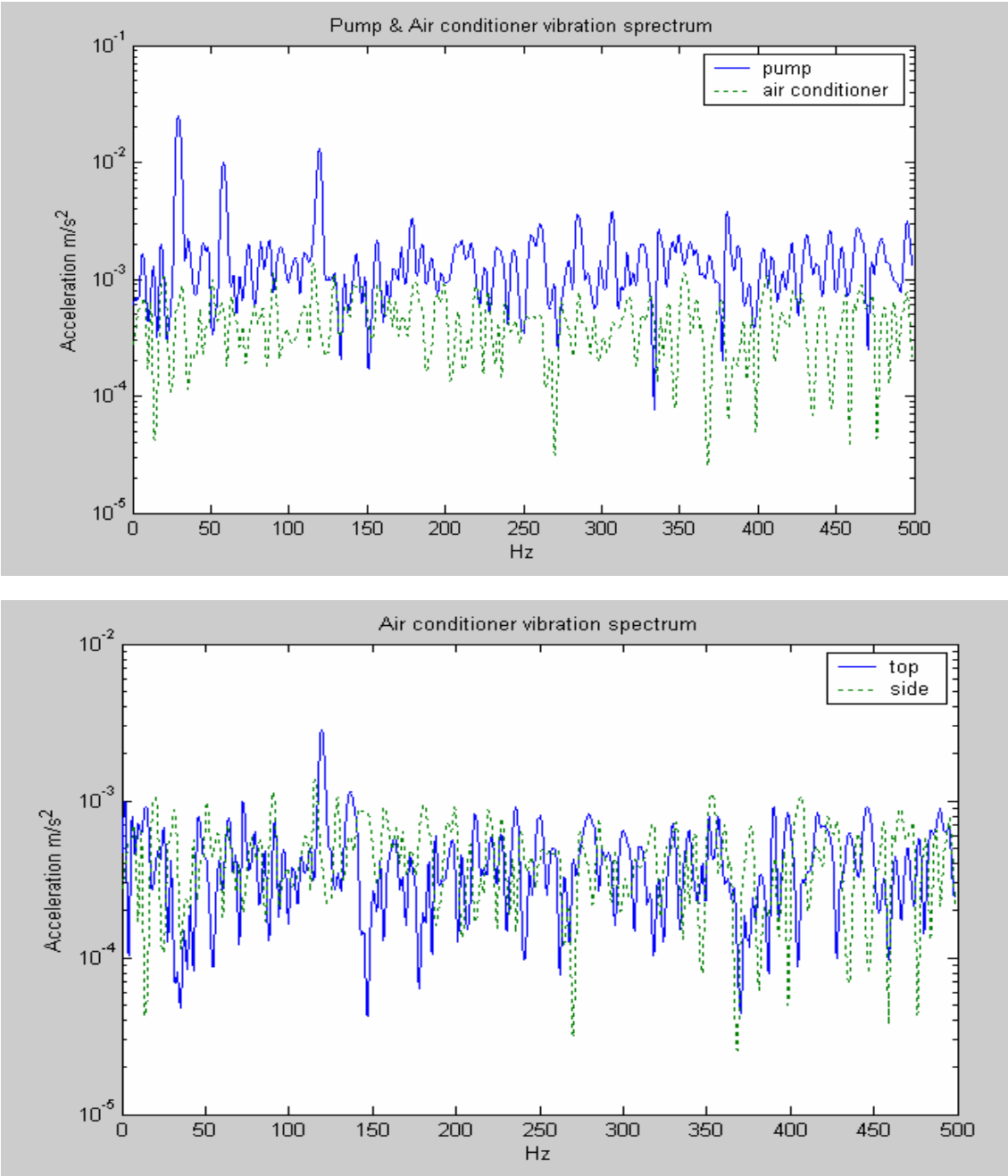

Figure 2.4 Vibration spectra of (a) pump and air conditioner (b) air conditioner

2.3 Device design

In device design, first the topology of the variable capacitor is explored. Next the dynamic analysis using analytical approximation with squeeze film damping effect taken into consideration is performed. Finally, optimal design parameters with numerical Simulink simulation are obtained.

From Equation 2.2, the output power is proportional to $(C_{max} - C_{min})(\frac{C_{max}}{C_{min}})$. Thus the main approach to increase P is to maximize the variation of the variable capacitance. Furthure more, it is desirable to target a fabtication process that can produce devices with large capacitances. A very thick device layer and a high aspect ratio are therefore necessary. This study takes advantage of the Silicone-On-Insulator (SOI) wafer in that it can offer very thick struecures (up to 500 μm or more). As for high aspect ratio, the deep reactive ion etching (Deep RIE) process is used to fabricate the devices with aspect ratio up to 20:1 .

2.3.1 Variable capacitor

For any capacitors, the capacitance can be varied by change the overlap area or the gap between electrodes. In the following sections, topologies of three types of micromachined variable capacitors are discussed: out-of-plane gap closing, in-plane overlap and in-plane gap closing. In Figures 2.5~2.7, the dark areas are structures fixed by anchors to the substrate, while the light areas are released structures that are free to move. A list of the symbols used in the following analysis is shown below.

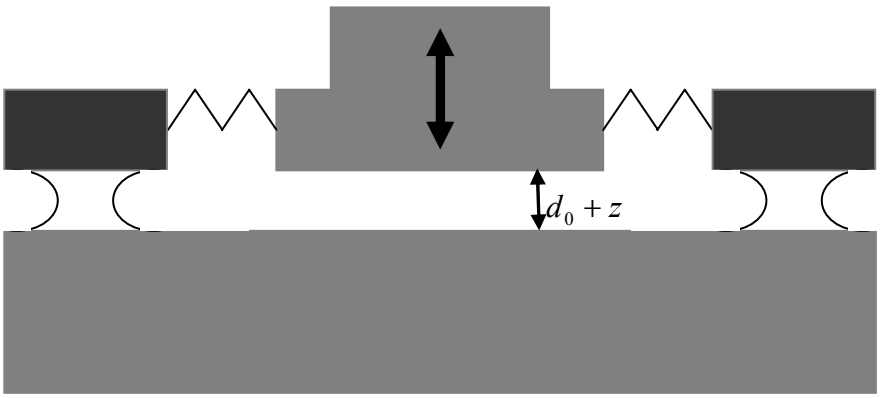

Figure 2.5 Cross-section of the out-of-plane gap closing type

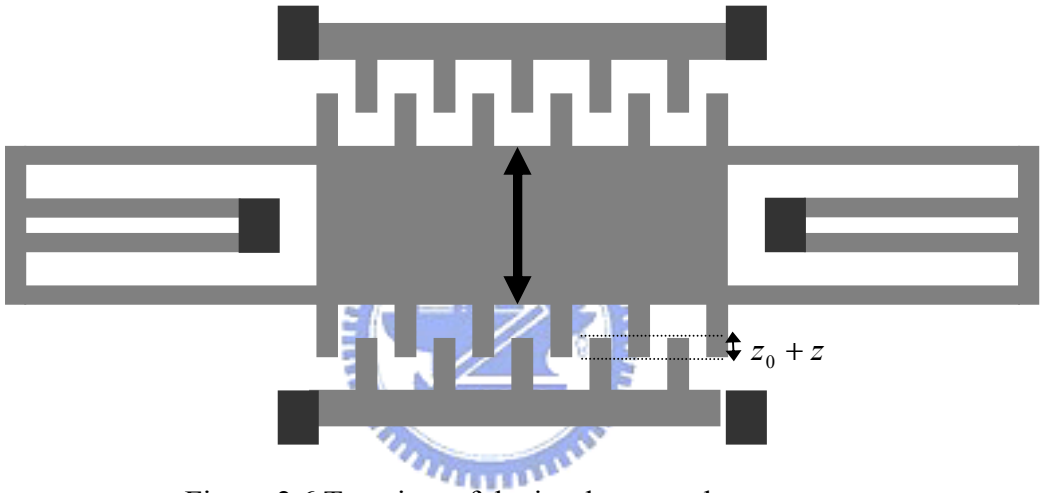

Figure 2.6 Top view of the in-plane overlap type

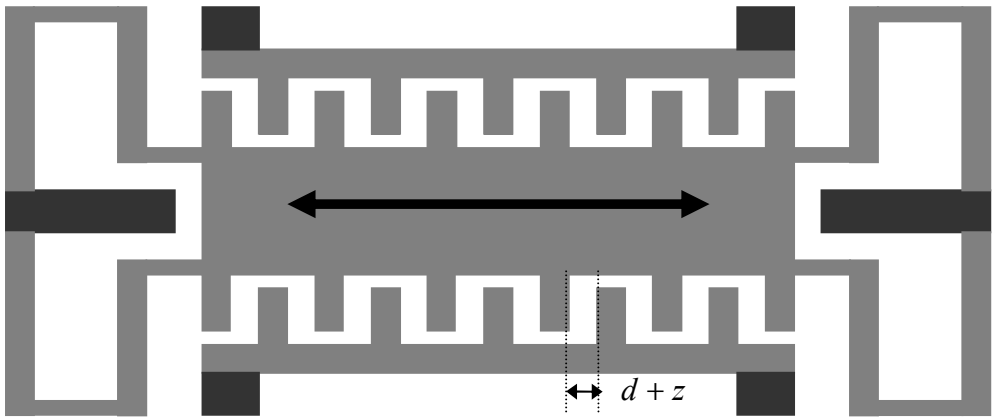

Figure 2.7 Top view of the in-plane gap closing type

A : top-view area of the movable plate,

d : initial gap between interdigitate fingers,

d_0 : initial gap between the top plate and the substrate,

L_f : length of comb fingers,

h : thickness of comb fingers,

N_g : number of gaps in the interdigitated comb fingers,

z : displacement of the movable plate,

z_0 : initial overlap length of interdigitated comb fingers,

W : width of the plate,

L : length of the plate.

1. Out-of-plane gap closing type:

The side view of an out-of-plane gap closing type variable capacitor is shown in Figure 2.5. The movable plate oscillates perpendicular to the substrate, and changes the capacitance by changing the dielectric distance between the top and bottom electrodes. The capacitance of the variable capacitor is

$$C_v = \frac{\varepsilon_0 WL}{(d_0 + z)} \tag{2.4}$$

where ε_0 is the permittivity of free space. Note that the interpretaion of z in this equation is slightly different from that in Figure 2.2. The sign of z is positive when the plates are moving apart, negative otherwise. The mechanical damping due to squeeze film damping is given by [21, 22]

$$b_m(z,\dot{z}) = \alpha(W/L)\frac{\mu W^3 L}{{d_0}^3}\frac{1}{(1-\varepsilon^2)^{-1.5}}\dot{z} \tag{2.5}$$

where $\alpha(W/L)$ is a coefficient related to the ratio of width and length,

$\mu = 1.82\times10^{-5}$ Pa-sec is the viscosity of air and is proportional to the

pressure, and $\varepsilon = \frac{z}{d}$ is the normalized displacement of the movable plate.

Finally, the electrostitc force is given by

$$b_e(z) = \frac{-Q^2}{2\varepsilon_0 WL}, \tag{2.6}$$

where Q is the charge on the variable capacitor and the minus sign indicates an attraction force.

According to Equation 2.4, the plates must be very close to each other and (d_0+z) becomes very small in order to obtain large change in capacitance. Nevertheless, the squeeze film damping effect of air is propotional to $\frac{1}{(d_0 + z)^3}$. The loss of energy by this mechanical damping becomes enormous for small gap distance. This problem may be alleviated somewhat by packaging the device under low pressure.

Another problem is that in pratical consideration, there should be a mechanical stop to prevent the two plates from shortage and the pull-in effect caused by the electrostatic force. However, it is difficalt to implement an out-of-plane mechanical stop in the fabrication process.

Finally, the capacitance ranges from 253 to 1770 pF for a 1cm^2 area constraint, assuming the initial gap d_0 is 2 μm and displacement z is ±1.5 μm. This value is larger than the in-plane overlap type but smaller than the in-plane gap closing type devices, which will be discussed in the following sections.

2. In-plane-overlap type:

Figure 2.6 shows the top view of an in-plane-overlap variable capacitor. The expressions of the capacitance C_v, mechanical damping b_m and electrostatic force b_e are given by

$$C_v = \frac{N_g \varepsilon_0 h(z_0 + z)}{d}, \tag{2.7}$$

$$b_m(z,\dot{z}) = \frac{N_g \mu L_f h}{z}\dot{z} \ , \tag{2.8}$$

$$b_e(z) = \frac{Q^2 d}{2N_g \varepsilon_0 h (z+z_0)^2} \ . \tag{2.9}$$

For large capacitance change, both h, z and N_g should be large and d should be as small as possible. If the aspect ratio h/d is 50, thickness is 200 μm, and displacement is 40 μm, the range of the variable capacitance is approximately 539~561 pF when z_0 is 1000 μm, or 44~66 pF when z_0 is 100μm, which is smaller than out-of-plane gap closing capacitor.

3. In-plane gap closing type:

As shown in Figure 2.7, the spring of the in-plane gap closing variable capacitor makes it easier to move in the direction of finger gaps. Compared to the out-of-plane gap closing type, the motion is now in the plane of the wafer and mechanical stops can be easily incorporated with standard fabrication processes. Therefore, the minimum dielectric gap and thus the maximum capacitance can be precisely controlled. The capacitance C_v, mechanical damping b_m, and electrostatic force b_e are given by:

$$C_v = N_g \varepsilon_0 L_f h\left(\frac{2d}{d^2 - z^2}\right) \ , \tag{2.10}$$

$$b_m(z,\dot{z}) = \left(\frac{\mu A}{d_0} + \alpha(W/L)\frac{\mu N_g L_f h^3}{d^3}\frac{1}{(1-\varepsilon^2)^{-1.5}}\right)\dot{z}, \tag{2.11}$$

$$b_e(z) = \frac{-Q^2 z}{2N_g d \varepsilon_0 L_f h} \ . \tag{2.12}$$

The mechanical damping is the sum of the lateral air drag force between the movable plate and substrate and the squeeze film damping force between interdigitate fingers. According to Equation 2.12, the electrostatic force is propotional to the

displacement of the movable plate. Therefore, it acts more like a negative spring than a damper. In order to get enough change in the variable capacitance, the thickness h should be large and the displacement z be close to the initial gap d. In our calculatoin, the variable capacitance can range from 50pF to 1250pF, larger than that of the in-plane overlap and out-of-plane gap closing capacitors.

Based on the above discussion, the in-plane gap closing capacitor is choosen due to the large capacitance change and system stability. In designing an in-plane gap closing capacitor, the number of finger gaps N_g should be maximized to obtain large capacitance change according to Equation 2.10. However, for limited chip area, increased number of gaps will result in the decrease of initail finger distance d and the variable capacitance. Calculated from equations 2.2 and 2.10, Figure 2.8 shows the power output as a function of initial gap distance, assuming the thickness is 200 μ m, the finger length and width are 1200 μm and 10 μm, the input voltage is 3.3 V, vibration frequency is 120 Hz, the parasitic capacitance be 10 pF, and the chip area size of 1 cm^2.

It can be seen that the initial finger gap has an optimal value of 25 μm, for a max power output of 32.4 μW. It should be noticed that the comparison above and the values of the capacitances calculated are based on the gemotry and capacitance equations only, the dampings and system dynamics are not taken into consideration. The damping equations are listed here for the system analysis and dynamic simulation in the following sections.

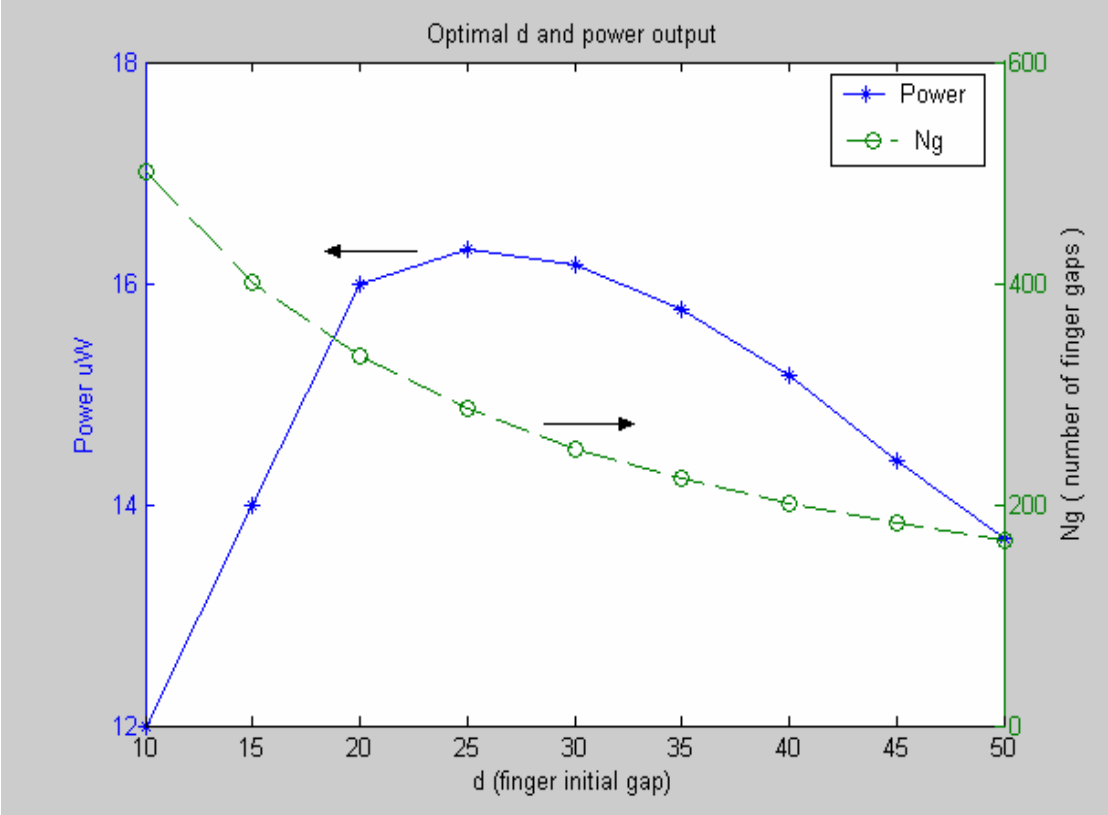

Figure 2.8 Output power vs. initial finger gap.

2.3.2 Dynamic analysis

Given the number of fingers and gap distance, the goal of dynamic analysis is to find the detail system design so that the movable plate can reach max displacement, and thus power output, under specific driving vibration conditions, which is 2.25 m/s^2 at 120 Hz as discussed in Section 2.2. The input voltage is assumed to be 3.3 V.

The SOI wafer used to fabricate the device has a device layer of 200μm, oxide layer of 2μm, handle layer (substrate) of 500μm. The minimum feature size is 10μm with consideration of the aspect ratio and perpendicularity of available Deep RIE processes. From Equations 2.3 and 2.10~12, the dynamic equation of the in-plane gap closing type converter can be written as

$$m\ddot{z} + \frac{-Q^2 z}{2N_g d\varepsilon_0 L_f h} + \alpha(W/L)\frac{\mu N_g L_f h^3}{d^3}\frac{1}{(1-\varepsilon^2)^{-1.5}}\dot{z} + kz = -m\ddot{y} \qquad (2.13)$$

Note that the drag force of air between the movable plate and substrate in the mechanical term is relatively small compare to the squeeze film damping effect between fingers (about 1:40 when z = 1.08 μm and 1: 4×10^6 when z = 24.5 μm), and thus can be neglected.

In fact, the squeeze film damping effect can behave like a damper at low frequency or turn into a spring at high frequency [23, 24]. The mechanical damping term of Equation 2.11 describe the damping behavior only. Thus, in order to be sure that the equation used in the model fits our requirement, Coventorware was used to check the values of the damping coefficient. As shown in Figure 2.9, the center finger moves in the direction of d. The simulation result shows the relationship between frequency and damping effect caused by the air squeezed in the fingers. It can be seen that the damping coefficient remains constant up to about 4000Hz and the simulation result agrees well with the calculation result from Equation 2.11. Since the application falls in the range of stable damping region, the assumption that the equation is reliable in this model is correct.

In Equation 2.13, both the Q and the ε are fucntion of z, therefore the system is nonlinear. In order to simplified the design, linear systems with fixed coefficients determined by the range of Q and ε are used to approximate the original system. Lapalace Transform is then applied to find the trend of system behaivor.

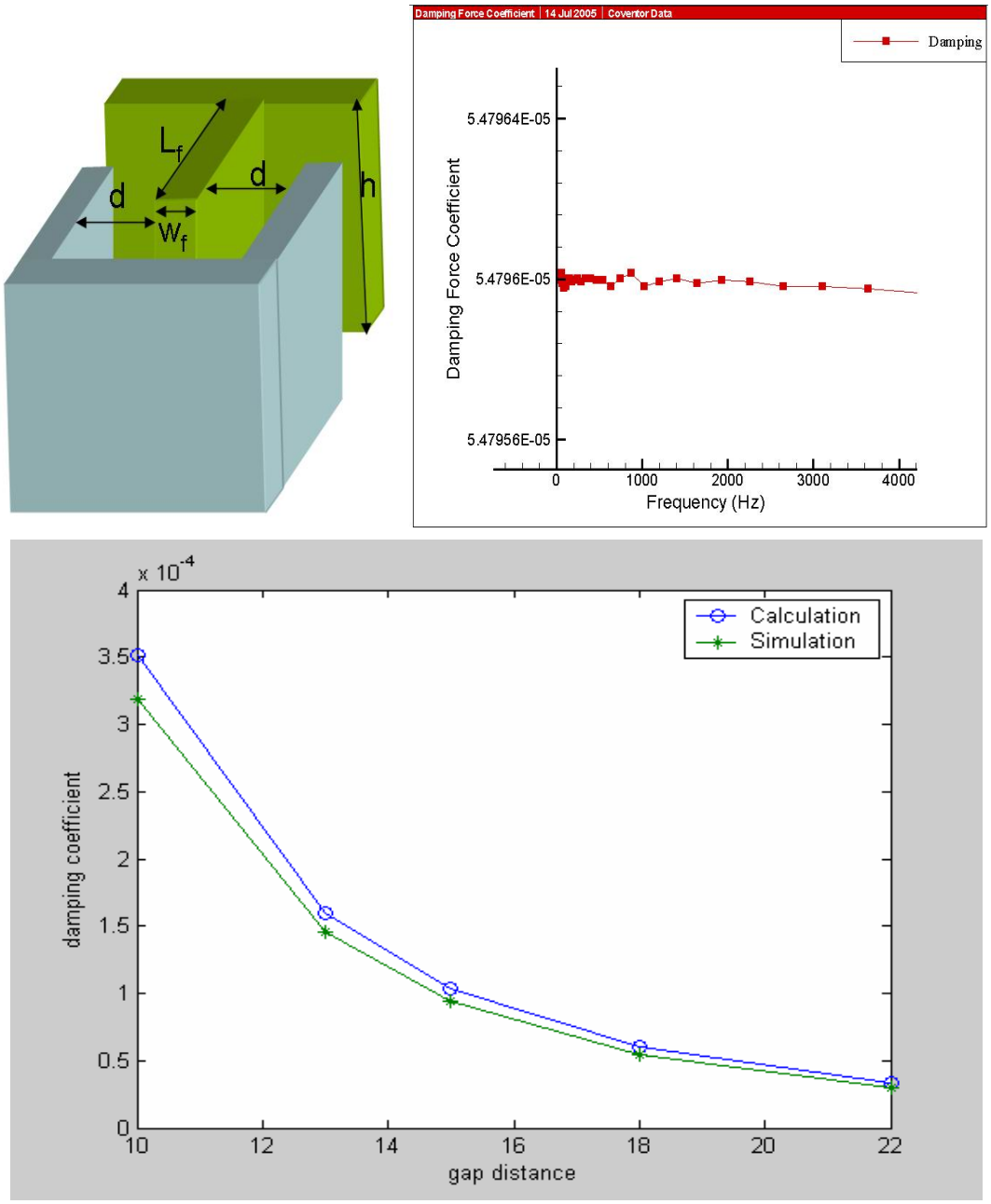

Figure 2.9 Squeeze film damping effect simulations

By Lapalace transform, the system response is

$$\frac{|Z|}{|Y|} = \left| \frac{S^2}{S^2 + \frac{\tilde{b}_m}{m} S + (\frac{\tilde{b}_e + k}{m})} \right| = \left| \frac{S^2}{S^2 + 2\zeta\omega_n S + \omega_n{}^2} \right| . \qquad (2.14)$$

The expected maximum defection Z = 24.5 μm and the amplitude of the vibration source Y were substitute into Equation 2.14. The $\tilde{b}_m$ and $\tilde{b}_e$ in Equation 2.14 are

asumed as $\tilde{b}_m = \alpha(W/L)\frac{\mu N_g L_f h^3}{d^3}\frac{1}{(1-\varepsilon^2)^{-1.5}}$, $\tilde{b}_e = \frac{-Q^2 Z}{2N_g d\varepsilon_0 L_f h}$ with Q asummed as $Q = C_{\max}V_{in} = N_g\varepsilon_0 L_f h(\frac{2d}{d^2 - Z^2})V_{in}$. The fixed parameters are d, h, N_g, V_{in} , W, and L. The denominator of the center part is devided into real and imaginary parts, where the real part $r = \frac{\tilde{b}_e}{m} + \frac{k}{m} - \omega^2$ is a funtion of L_f, k and m and the imaginary part $i = \frac{\tilde{b}_m}{m}$ is function of L_f and m. Assume that the real part r can be adjusted to zero by tuning k , thus we get a range of $L_f/m = 2.66\times10^7 \sim 2.09\times10^5$ μm/Kg by sloving the left half part of Equation 2.14 with the normalized displacement $\varepsilon = z/d$ varied from 0~24.5/25, and $k/m = 2.45\times10^7 \sim 7.56\times10^5$ μN/(μmKg) can be obtained by setting the real part to zero.

In the meanwhile, if the damping constant ζ is not large enough, overshoot will occur and the displacement will exceed the maximum allowable distance. This will result in the collision of the movable plate and the mechanical stops and cause the energy loss and system instability. Therefore higher damping ratio is preferred.

Larger comb finger length L_f will result in larger capacitance variation but also increase the mass needed to attach on the device. With the consideration of aspect ratio, length to width ratio and the robustness of fingers, 1200 μm was chosen. For L_f = 1200 μm, the values of $m \approx 4.5\times10^{-5} \sim 5.7\times10^{-3}$ Kg, $k \approx 1112 \sim 4315$ μN /μm are obtained. Those values will be used in the simulation in next section.

2.3.3 Simulations and parameter optimization

Through the above analysis, a rough range of parameters is obtained. In order to analyze the nonlinear system more accurately, Simulink is used to perform the dynamic simulation.

The block diagram of the dynamic simulation is shown in Figure 2.10. The

redistribution of charge is modeled based on the circuit schematic in Figure 2.1b. The contact detection block detects weather the displacement reaches the mechanical stop or not. The pull-in detection block checks if inertial force on the plate can separate the fingers when contact occurs. The parameters from the analysis above can be substituted into the Simulink model to find the response of the system. The change in variable capacitance is also observed. The exact Simulink model is shown in Appendix.

Figure 2.11 shows the maximum displacement of the movable plates with different mass attached. The corresponding spring constant which generates the maximum z are also showed. With larger mass it should be easier to reach the maximum displacement; however, under the size constraint of $1cm^3$, mass more than 19 gram is impractical even if tungsten is used. Actually, mass larger than 7 gram is hardly available. Thus through the iteration as shown in Figure 2.11, optimal design is obtained in Table 2.1 with m = 5.7Gram and k = 2.8kμN/μm. The output power under 3.3 V input is 32.34 μW, which is higher than the current results in literatures.

Figure 2.12 and 2.13 show the simulation result of displacement response and output voltage with the parameters in Table 2.1 for the vibration source of 2.25 m/s^2 at 120 Hz. The displacement reaches its maximum 24.5 μm in 0.02 seconds. The output voltage on the storage capacitor shows a charge pump like phenomenon and will mount to 83V if no charge is removed form the storage capacitor.

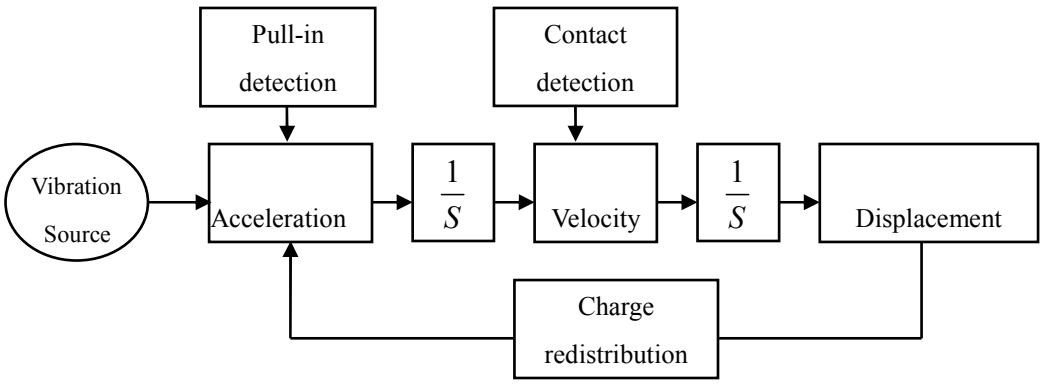

Figure 2.10 Dynamic simulation frame

Table 2. 1 Optimal design parameters

Variable	**Description of variables**	**0.5μm minimum gap**
W	Width of shuttle mass	10mm
L	Length of shuttle mass	8mm
L_f	Length of finger	1200μm
W_f	Width of finger	10μm
m	Shuttle mass	5.7Gram
d	Finger gap	25μm
d_0	Shuttle mass to base distance	2μm
k	Spring constant	2.8kμN/μm
V_{in}	Input voltage	3.3V
C_{min}/C_{max}	Min/Max capacitance	50 / 1250 pF
Pout	***Output power***	***32.34μW***

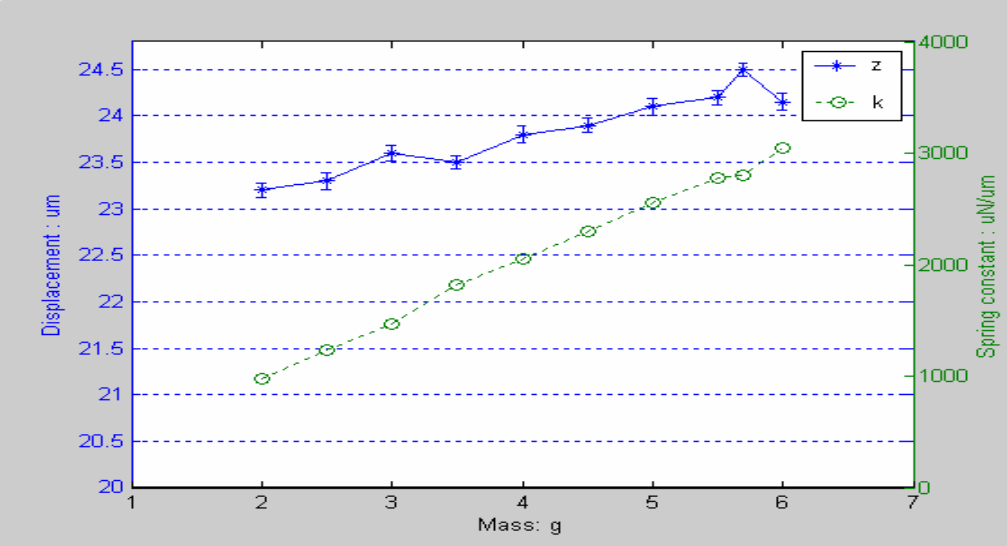

Figure 2.11 Max displacement *z* and spring constant *k* for various attached mass *m*

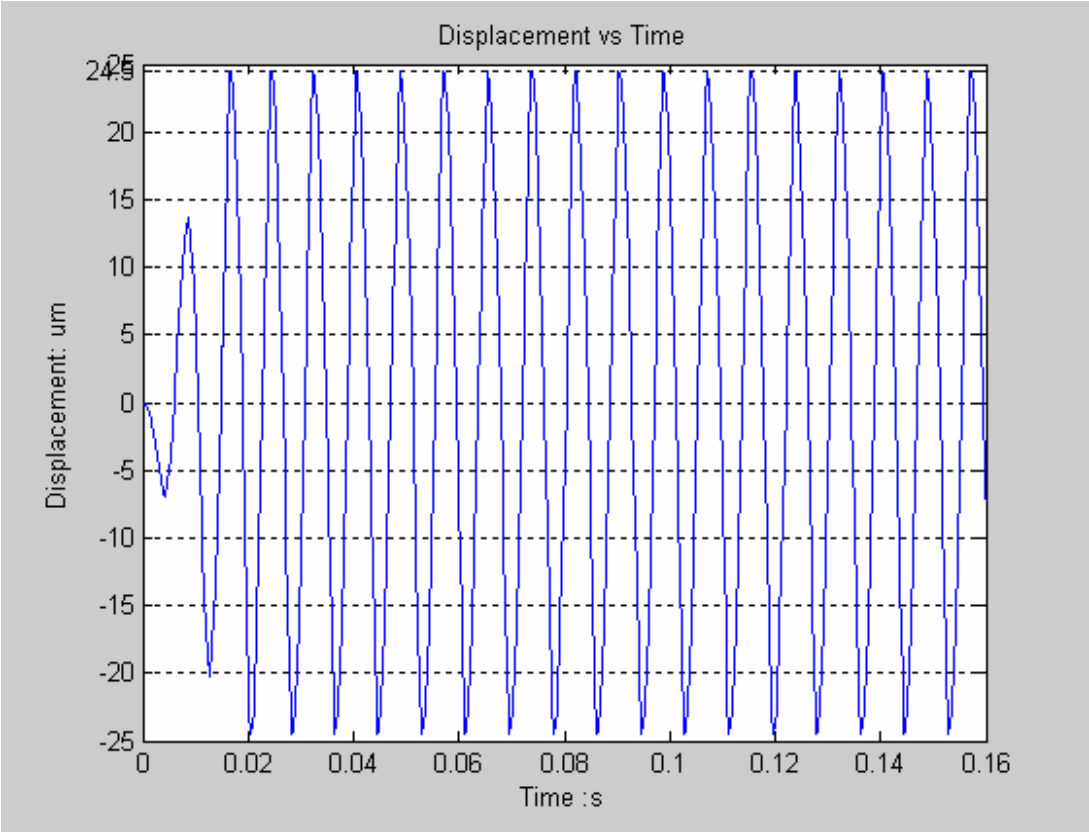

Figure 2.12 Simulation of displacement Z

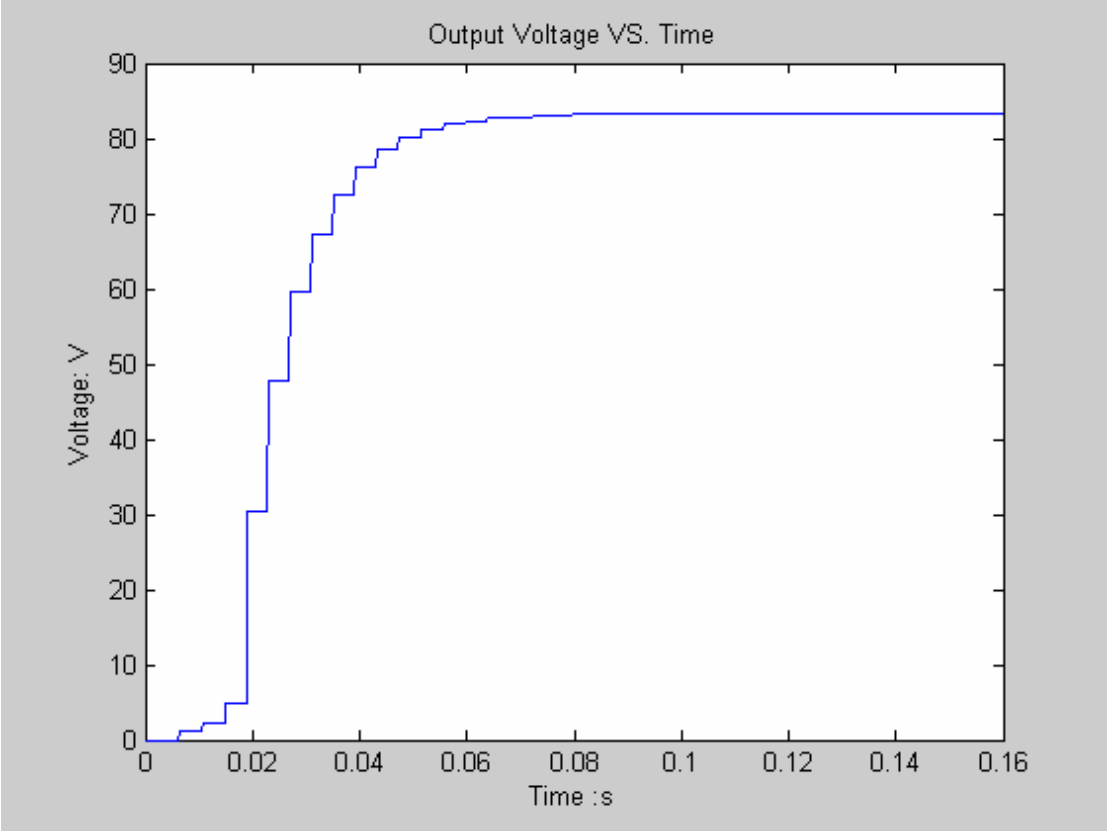

Figure 2.13 Simulation of output voltage Vo

2.4 Spring design

According to the dynamic analysis in the previous section, two important parameters are decided: the shuttle mass *m* and the spring *k*. The shuttle mass is 5.7 gram, which is relatively huge in MEMS and can be hardly fabricated even using SOI wafers. As a result, a high density material such as tungsten (W) or steel should be attached to adjust the mass.

Since the shuttle mass is extraordinary large, the out of plane elasticity can influence the reliability of the system. For the spring structure in Figure 2.14, the spring constants in the three axes are [11, 25]:

$$K_z = N\frac{Eh^3W_k}{2L_k^3}, \tag{2.15}$$

$$K_x = N\frac{EhW_k^3}{2L_k^3}, \tag{2.16}$$

$$K_y = N\frac{EhW_k}{2L_k}, \tag{2.17}$$

where N is the number of folded springs,

h is thickness of spring, (=200 μm)

E is the young's modulus of single crystal silicon,(=169GPA),

L_k and W_k are the length and width of spring

Since the spring thickness h and Young's modulus E are fixed, only the spring length, width, and number of springs can be altered to achieve the desired stiffness. Incidentally, more than four folded spring should be incorporated.

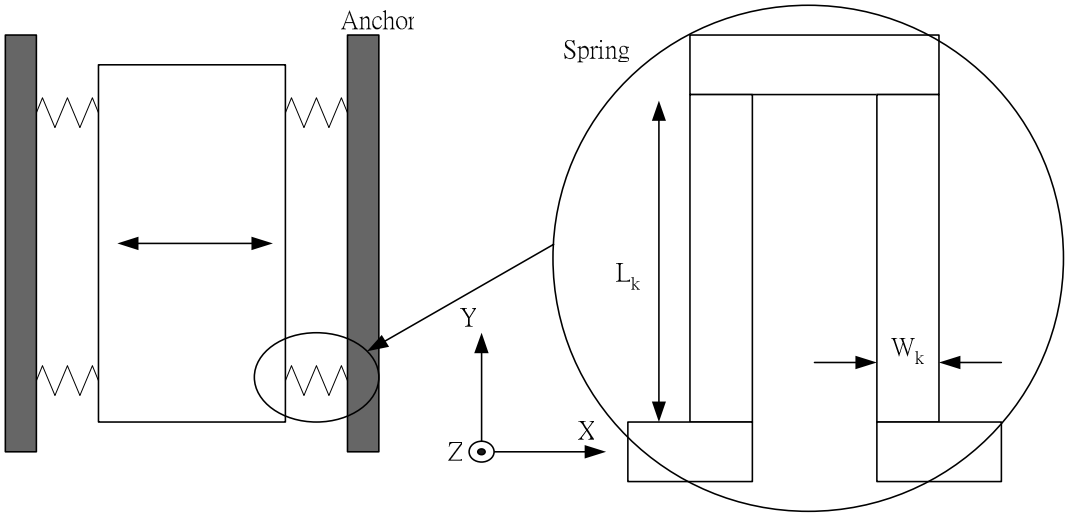

Figure 2.14 Spring structure top view

Several issues should be considered. First, the vertical stiffness K_z should be at least 10 times lager than the lateral stiffness K_x to reduce out-of-axis motion. The static displacement under the weight of the proof mass, mg/K_z, is also important. Second, the yield stress for single crystal silicon is about 70 GPa. A safety factor Sf defined as the yield stress divided by the maximum stress on each axis will be helpful in checking the robustness of the spring. The maximum stress due to the lateral displacement and the static vertical loading of the proof mass are given

$$\sigma_x = \frac{3EW_k x_{\max}}{2L_k^{\,2}} \tag{2.18}$$

$$\sigma_z = \frac{3mgL_k}{NW_k h^2} \tag{2.19}$$

where x_{max} is the maximum lateral displacement

The final designed parameters of the springs are listed in Table 2.2. There are 6 springs as shown in Figure 2.15, on each side of the shuttle plate and the resonant frequency is 111 Hz. The maximum lateral stress is 0.37 GPa where the maximum displacement is 24.5 μm. The maximum vertical stress is 15.15 GPa with mass m = 5.7 g. The K_x is 2800μN/μm which is far below the other two spring constant.

Table 2. 2 Spring design and safety factor.

Variable	Description of variables	Thickness 200 μm
N	Spring number	12
W_k	Spring Width	10 μm
L_k	Spring Length	433.5μm
K_z	Vertical spring constant	1.12 M μN/μm
K_x	X-axis spring constant	2800 μN/μm
K_y	Y-axis spring constant	5260 KμN/μm
K_z / K_x	Vertical to lateral spring ratio	400
K_y / K_x	Non-axial to axial spring ratio	1879
Sf_x	Safety factor – axial	188.39
Sf_z	Safety factor – vertical static	4625.2

Modal analysis is performed by Coventorware. The result shows that the first mode of resonant is at 93 Hz and the direction is lateral. The second mode is 233 Hz and the movable plate moves in tilt direction. The second mode frequency is more than twice of that of the first mode, which is quite safe in this application. The equivalent lateral spring constant (1970 μN/μm) is smaller than calculated. However, the shift in resonant frequency due to spring modeling can be adjusted by adjust the external load mass.

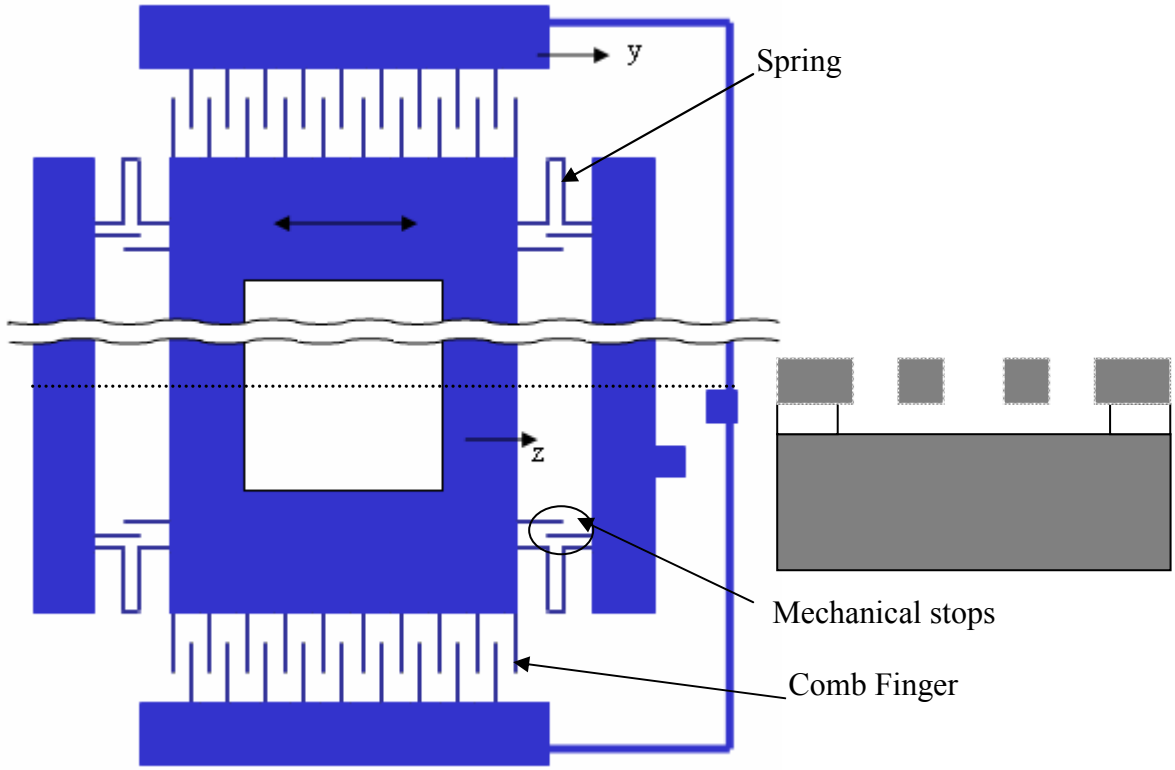

Figure 2.15 Schematic and cross-section of device

2.5 Discussion

The overall schematic is shown in Figure 2.15. The mechanical stops are designed both on the plate and the anchor. The fixed fingers are electrically connected. For the design shown in Table 2.1, the maximum lateral displacement is 24.5 μm. The center hole on the movable plate is for the positioning of the attached mass, a steel ball. The size of the center hole is designed to keep the ball from touching the substrate beneath.